Lasers in Manufacturing Conference 2021

Influence of process-relevant parameters and heat treatments on the microstructure and resulting mechanical behavior of additively manufactured AlSi10Mg via Laser Powder Bed Fusion

Andreas Kempf[a*], Leonardo Agudo Jácome[b], Kai Hilgenberg[b]

[a]*Volkswagen Aktiengesellschaft, Brieffach 14370, 38436 Wolfsburg, Deutschland*
[b]*Bundesanstalt für Materialforschung und –prüfung (BAM), Unter den Eichen 87, 12205 Berlin, Deutschland*

Abstract

Within the group of additive manufacturing (AM) technologies for metals, laser powder bed fusion (L-PBF) has a leading position. Nevertheless, reproducibility of part properties has not reached sufficient maturity hindering the use for industrial applications especially for safety-relevant components. This article presents the results of various experimental tests performed with the aluminium alloy AlSi10Mg identifying reasons for the high deviations in mechanical properties. Herein, it is discussed how microstructure is influenced by different process parameters (laser power, scanning speed, energy density, building height) and how it can be adjusted by suitable post process heat treatments. The impact of resulting changes in microstructure is shown by monotonic tensile and cyclic fatigue tests considering specimens manufactured with different L-PBF machines.

Keywords: Additve manufacturing; Laser powder bed fusion; AlSi10Mg; Microstructure; Mechanical behavior

1. Introduction

L-PBF is an additive AM technology in which parts are built up line-by-line and layer-by-layer. Doing this, a laser melts a powdery raw material following a computer aided model. This allows the production of components with almost unlimited geometrical freedom, but requires long manufacturing times. Due to the tool-less production, manufacturing capacity can be increased by working with multiple L-PBF machines. In order to realize such a parallel production of components it has to be ensured that the same part quality, for

* Corresponding author. Tel.: 05361-9-990523.
E-mail address: andreas.kempf1@volkswagen.de.

instance in terms of dimensional accuracy and tolerances, surface quality, corrosion resistance, mechanical properties, and microstructure, can be obtained from different L-PBF systems. At this background, the present work provides an experimental based overview about the interactions between process parameters, microstructure, and mechanical behavior of AlSi10Mg specimens processed with different L-PBF instruments and heat treatments.

2. Experimental setup

Three different types of L-PBF systems were used for specimen fabrication. Table 1 summarizes the machine types, the process parameters, the built-up strategies, and the particle sizes of the AlSi10Mg powders. The specimens` geometry manufactured for each objective are illustrated in Fig. 1 including the building direction, the applied L-PBF machines, and the preparation planes for metallographic examinations. Microstructure was analysed via optical light microscopy (Zeiss, AX Imager. A2), scanning electron microscopy (SEM, Zeiss Supra 40 VP) operating with an in-lens detector, and transmission electron microscopy (TEM, JOEL JEM 220FS) working in scanning (S)TEM bright field (BF) and dark field (DF) mode, respectively. Additionally, energy dispersive spectrometer (EDS) analysis were performed in STEM mode. Vickers hardness testing HV1 (DuraVision 20) was conducted at section planes, which are perpendicular to the specimens` building direction, with five indentations per plane. Monotonic tensile tests (Zwick, Z250 SW) were performed according to DIN EN ISO 6892-1 standard at room temperature with a strain rate of 0.006 s^{-1} considering five measurements for each batch. Cycle fatigue tests were carried out according to DIN 50113 at room temperature on a rotating bending machine (Walter + Bai UBM 200 Nm). A testing frequency of 60 Hz and a stress ration of R = -1 were used. High cycle fatigue (HCF) tests were terminated at 10^7 cycles. Mechanical properties were determined in the as-built condition, annealed heat treated (300 °C/ 2 h), and T6 heat treated (525 °C/ 2h – water quenching – 160 °C/ 8 h).

Table 1. Standard parameter settings of the three L-PBF machines

	Machine A	Machine B	Machine C
Machine type	SLM 280 HL	SLM 500	Concept Laser XLine 2000R
Particle size of powder D_{10}, D_{50}, D_{90} in µm	24, 38, 60	27, 39, 54	41, 56, 71
Laser power P_L in W	700	350	950
Scanning speed v_S in mm/s	2260	1650	2450
Layer thickness d in µm	50	30	60
Hatch distance y in µm	170	130	180
Temperature of building platform in °C	150	150	200
Build up strategy	Stripes (10 mm), 67°-alternating	Stripes (10 mm), 67°-alternating	Stripes (10 mm), 90°-alternating

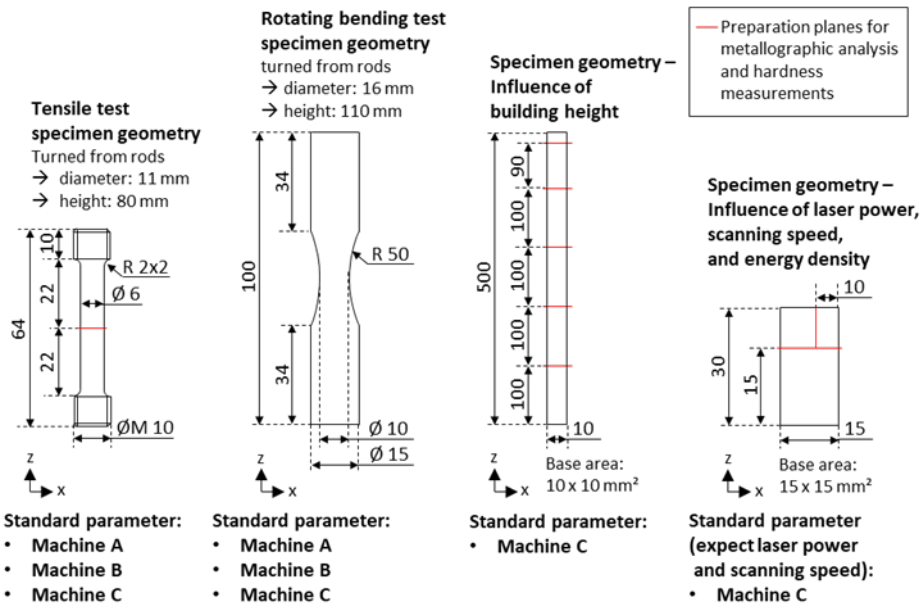

Fig. 1. Specimens` geometry, building direction, and preparation planes for metallographic analysis.

3. Results and Discussion

3.1. Monotonic tensile properties and microstructure from different L-PBF machines in the As-built condition

Fig. 2a summarizes the monotonic properties from tensile tests of the three L-PBF machines after the manufacturing process. It can be clearly seen that the mean values of the mechanical characteristics show a large variance: The difference to the highest mean value in the ultimate tensile strength, yield strength, and elongation at fracture is of the order of 29%, 22%, and 65%, respectively. The deviations of monotonic strength

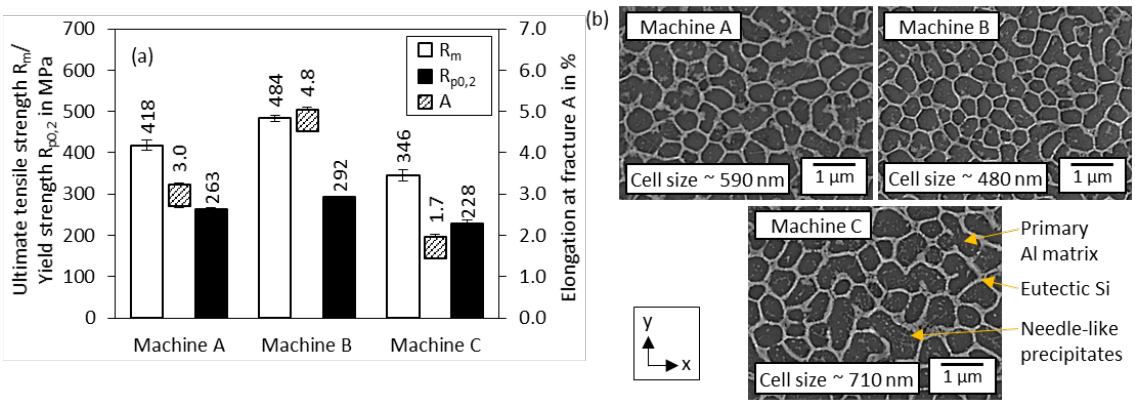

Fig. 2. (a) Monotonic tensile properties and (b) SEM microstructure of the three L-PBF machines in the as-built condition.

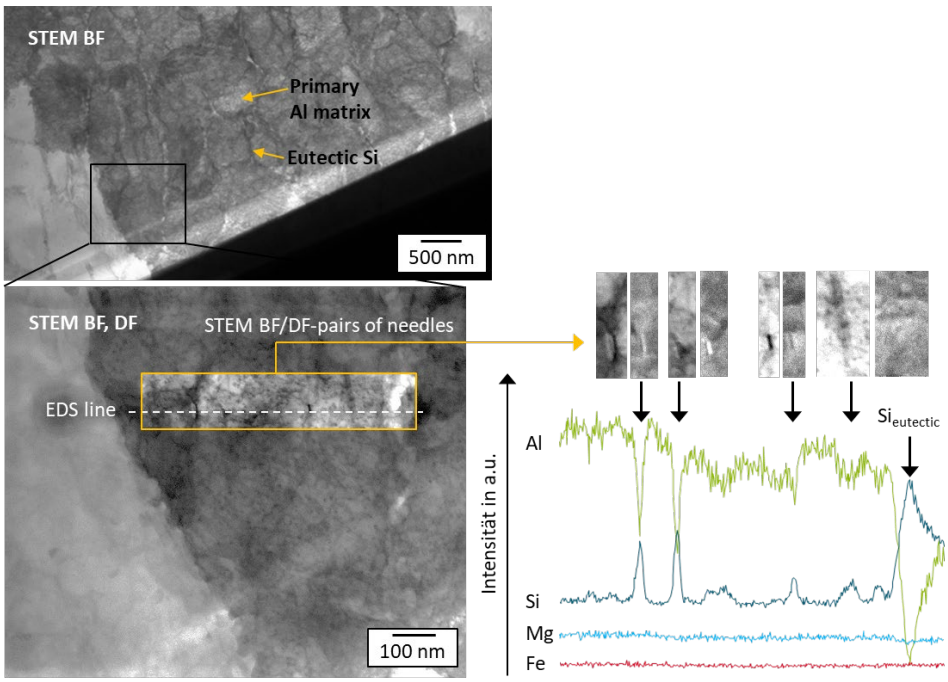

Fig. 3. STEM BF and DF images including EDS mapping of a specimen manufactured with L-PBF machine C (standard parameter).

properties can be traced back to the microstructural differences. L-PBF processed AlSi10Mg typically consists of a sub-cellular network which is composed of primary Al (dark areas in SEM analysis) and eutectic Si (bright areas in SEM analysis) and Al phases [1]. A comparison of these features of the three L-PBF machines in Fig. 2b reveals that a refining of the sub-cells correlates with a higher monotonic strength. Since the separated eutectic Si particles of the sub-cell boundaries act as precipitates which are passed by Orowan looping mechanism during the dislocation movement [2], increased monotonic strength of specimens with smaller sub-cells can be explained by precipitation strengthening mechanism [3].

As a further microstructural conspicuousness, tinny needle-like precipitates within the primary Al can be observed (Fig. 2b). Because their composition was not determinable using SEM-EDS, TEM-EDS analyses were performed showing that they are of pure Si (Fig. 3).

An overall view of the results in this Section raises the following questions:

- Can the sub-cell size adjusted by important process parameters (scanning speed, laser power, energy density) ? → see *Section 3.2.*
- How is the formation mechanism of the needle-like precipitates? see *Section 3.3.*
- Can microstructural differences be homogenized by post-process heat treatments? How is the impact on the mechanical performance? → see *Section 3.4.*

3.2. Influence of laser power, scanning speed, and linear energy density on the microstructure

The effect of the scanning speed and laser power on the hardness is illustrated in Fig. 4a. For a constant laser power, hardness is reduced with decreasing scanning speed. For a constant scanning speed, hardness is reduced with increasing laser power. These findings can be explained considering the energy input. A decrease

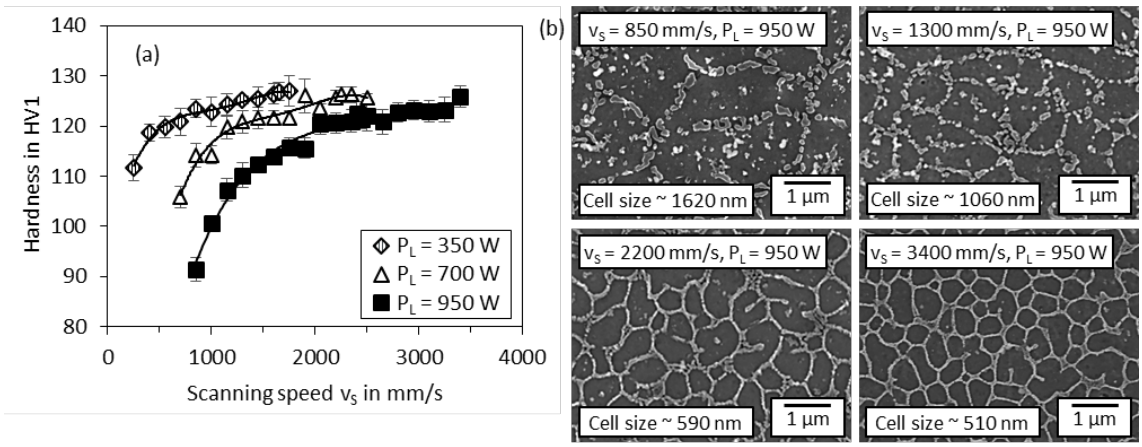

Fig. 4. (a) Hardness evolution in dependence of scanning speed and laser power, (b) microstructure (xy plane) evolution in dependence of scanning speed for a laser power of P_L = 950 W.

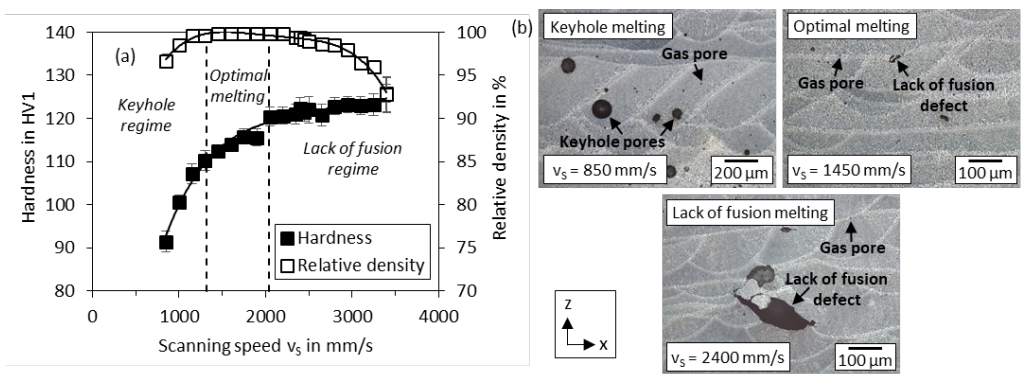

Fig. 5. (a) Hardness evolution in dependence of scanning speed and laser power, (b) microstructure (xy plane) evolution in dependence of scanning speed for a laser power of P_L = 950 W.

of the scanning speed and an increase of the laser power lead to a higher energy input (linear energy density), respectively. Thus, the volume of molten material increases which results in a higher cooling time. This, in turn, causes a coarsening of the microstructure (sub-cell structure, Fig. 4b) with the detected drop in hardness.

However, it should be noted that parts manufactured with L-PBF always exhibit a certain amount of porosity. There are three main types of material defects: keyhole pores, gas pores, and lack of fusion defects [4]. Gas pores arise from trapped gases in the melt pool or from evolved gases from the powder feedstock [4]. As depicted in Fig. 5, keyhole pores are formed at low scanning speeds (high energy density) due to over-melting, and lack of fusion defects are created at high scanning speeds (low energy density) due to under-melting. Finally, this is the reason why the processing region of the maximum hardness does not correspond with the processing region of the maximum density (Fig. 5a). Hence, finding optimal parameters is connected with a compromise between hardness and density. Additionally, since the optimal melting region is in a narrow range of scanning speeds (for a defined laser power), adjusting the sub-cell size and , thus, the tensile strength properties is further limited.

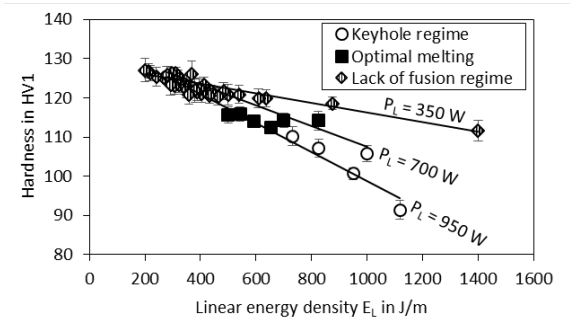

Fig. 6. Hardness evolution in dependence of linear energy density for different P_L-v_S-combinations.

For the L-PBF process it would be promising, if a value for the energy input could be defined to work with reaching a microstructure with specific mechanical properties. To point this out, hardness evolution in dependence of the linear energy density for different P_L-v_S-combinations is plotted in Fig. 6. Considering a constant linear energy density, two observations can be made: Firstly, with increasing linear energy density the range in hardness is increased for different P_L-v_S-combinations. Secondly, different types of material defects are formed for different P_L-v_S-combinations. Therefore, it is to conclude that the linear energy density does not reflect the actual heat input during the melting processes and is an unsuitable parameter to predict the microstructure. A possible reason is that the thermal history of the already molten material is not taken into account in the value of the linear energy density. If a constant linear energy density is assumed, then, a higher laser power is connected with a higher scanning speed. That means that the previously manufactured laser tracks and layers have less time for cooling so that the temperature gradient decreases. As a consequence, the volume of the molten material is increased. This is supported by the different identified material defects and most evident for a linear energy density of E_L = 825 J/m: A laser power of P_L = 350 W resulted in lack of fusion defects (under-melting), a laser power P_L = 700 W led to a maximum in density (optimal melting), and a further increase of the laser power to P_L = 950 W created keyhole porosity (over-melting). Another effect of a reduced temperature gradient is a coarsened microstructure. This causes lower hardness which is in agreement with the conducted measurements.

3.3. Influence of building height on the microstructure

As it can be seen in Fig. 7a, the mean values of the sub-cell size show no significant changes in the examined building heights. Nevertheless, a hardness gradient of approximately 15% was obtained, in which hardness is reduced downwards the part height. Representative SEM images in Fig. 7b demonstrate increasingly more needle-like precipitates (Si) within the primary Al matrix in the lower building heights. Due to the long building time of the specimens, these observations can be seen as an evidence that Si particles, which were originally retained in solid solution upon the melting process, were precipitated out from the Al matrix caused by an in-situ heat treatment through the manufacturing process itself. Consequently, microstructure is not necessarily influenced by the building height in these experiments, but rather by the manufacturing time and the occurring temperatures. However, there are different findings of the impact on the mechanical properties. Fousová et al. found an increase in the yield strength of 5%, whereas the ultimate tensile strength and elongation at fracture decreased by 9% and 60%, respectively [5]. The authors in Ref. [6] documented a drop in the yield and ultimate tensile strength of 10% and 7%, respectively, without a significant change of the elongation at fracture.

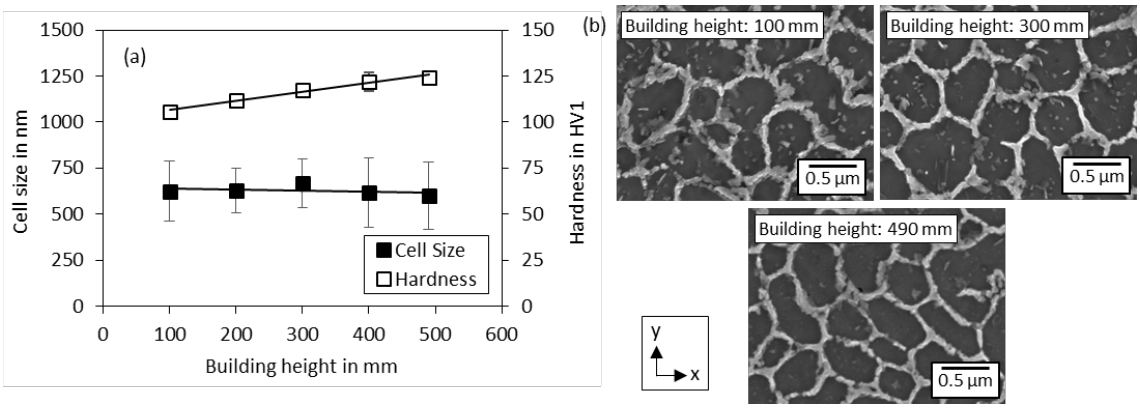

Fig. 7. (a) Sub-cell size and hardness evolution in dependence of build height, (b) SEM microstructure in different build heights.

3.4. Monotonic tensile and cyclic properties from different L-PBF machines after heat treating

Fig. 8 illustrates the monotonic tensile properties of the three L-PBF machines after an annealing and T6 heat treatment, respectively. Compared to the As-built manufactured specimens, differences in the monotonic strength properties were leveled out almost completely for both procedures indicating a homogenization in the microstructure. Thereby, the annealing heat treatment decreased considerably the ultimate tensile and yield strength to 265-272 MPa and 142-162 MPa, respectively. The T6 heat treatment also reduced the ultimate tensile strength for all L-PBF machines to 302-311 MPa, but an improvement of the yield strength can be reached ($R_{p0,2}$ ~ 242-248 MPa). Nevertheless, appreciable differences in the elongation at fracture remained for the different L-PBF machines.

A comparison of representative stress-strain and S-N curves for T6 heat treated specimens with turned surface finish is given in Fig. 9. The fatigue strength in the low cycle fatigue (LCF) regime does not differ significantly between the three L-PBF machines and corresponds approximately with the yield strength. In contrast, the differences in the fatigue strength in the HCF regime are up to 40% and show a correlation with the differences in the elongation at fracture. Due to the fact that monotonic properties are “global” and cyclic strength depends on “local” features, the question arises how this relationship can be justified. It is well known for L-PBF processed AlSi10Mg that ductility is reduced with an increasing amount of material defects [6], and

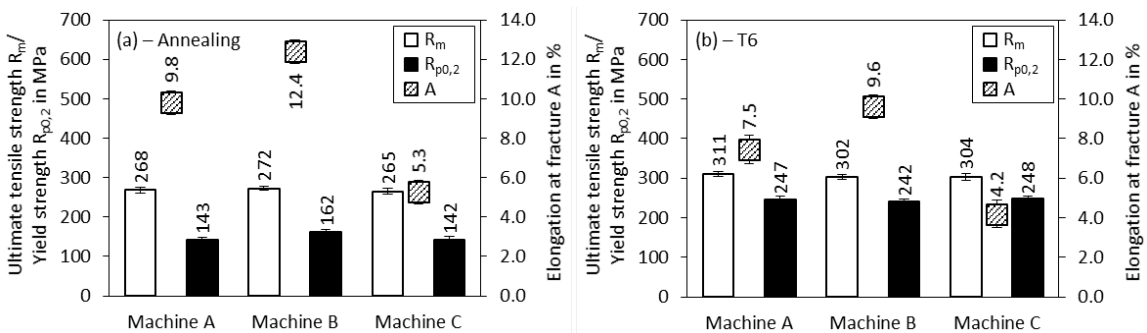

Fig. 8. Monotonic tensile properties of the three L-PBF machines after (a) annealing and (b) T6 heat treating.

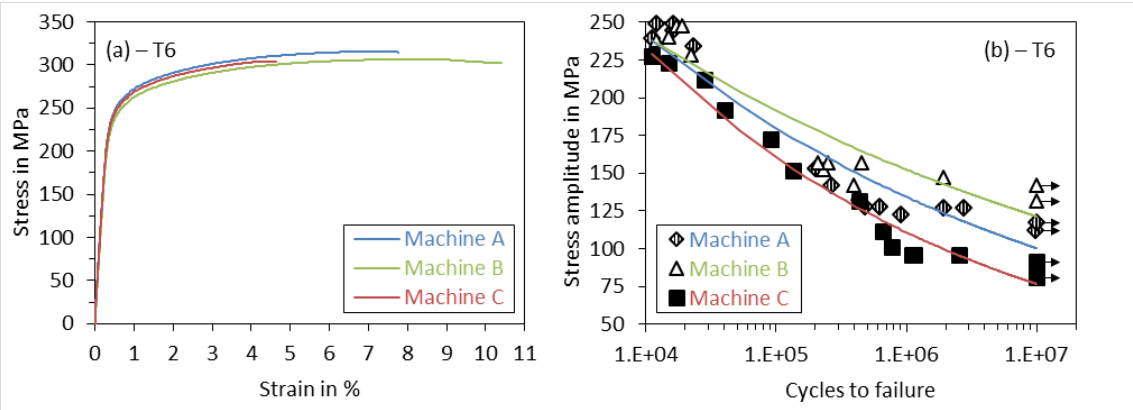

Fig. 9. (a) Representative stress-strain curves and (b) S-N curves for T6 heat treated specimens of the three L-PBF machines.

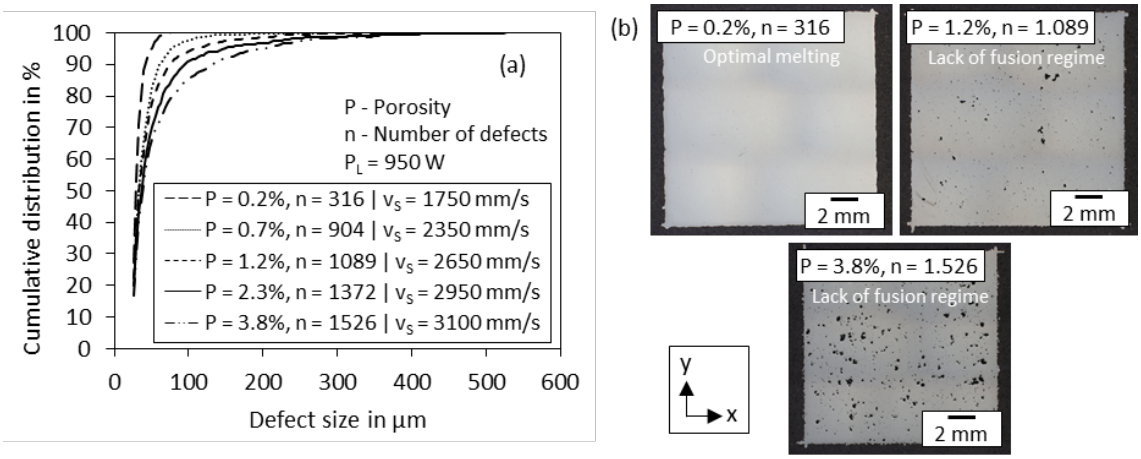

Fig. 10. (a) Cumulative defect size distribution in dependence of porosity and number of defects and (b) optical light images used for corresponding measurements – representative specimens of process parameter study analysed in Section 3.2 (L-PBF machine C).

fatigue strength of L-PBF materials is strongly affected by the size of individual defects [7]. Therefore, the correlation between the elongation at fracture and fatigue strength can be explained by the fact that a higher porosity in a L-PBF material is related to both an increase in the number and size of pre-existing, within the total part volume distributed material defects. This is verified in Fig. 10 showing the results of porosity measurements for different parameter combinations in the optimal melting and lack fusion regime, respectively.

4. Conclusions

In this work, the influence of process parameters and heat treatments on the microstructure and mechanical properties of L-PBF processed AlSi10Mg was investigated. The following conclusions can be drawn:

- The monotonic strength properties in the As-built condition correlates with the size of the microstructural sub-cell network resulting in high deviations for different L-PBF machines.

- A variation of laser power and scanning speed can change the size of the sub-cells, respectively. Nevertheless, a specific adjustment of a fine-sized microstructure with high strength is limited, since porosity increases dramatically with decreasing sub-cells size and the optimal melting region (maximum density) is in a narrow range of scanning speeds.
- The linear energy density is not a reliable parameter for material synthesis by L-PBF, since the cooling conditions are affected by the previously exposed laser tracks and layers.
- Building time can cause a gradient in microstructure and hardness over the part height. However, monotonic strength properties seems to be affected only marginal.
- Different heat treatments are able to homogenize microstructure for the used process parameters and monotonic strength properties. Nevertheless, appreciable differences in the HCF strength were determined.
- A correlation between the elongation at fracture and HCF strength has been observed which is caused by the presence of material defects.

References

[1] Lam, L.P., Zhang, D.Q., Liu, Z.H., Chua, C.K., 2015. Phase analysis and microstructure characterisation of AlSi10Mg parts produced by Selective Laser Melting, Virtual and Physical Prototyping 10:4, p. 207-2015.

[2] Chen, B., Moon, S.K., Yao, X., Bi, G., Shen, J., Umeda, J. Kondoh, K., 2017. Strength and strain hardening of a selective laser melted AlSi10Mg alloy, Scripta Materialia 141, p. 45-49.

[3] Kempf, A., Hilgenberg, K., 2020. Influence of sub-cell structure on the mechanical properties of AlSi10Mg manufactured by laser powder bed fusion, Material Science & Engineering A 776, p. 138976.

[4] Aboulkhair, N.T., Everitt, N.M., Ashcroft, I., Tuck, C., 2014. Reducing porosity in AlSi10Mg parts processed by selective laser melting, Additive Manufacturing 1-4, p. 77-86.

[5] Fousová, M., Dvorský, D., Michalcová, A., Vojtěch, D., 2018. Changes in microstructure and mechanical properties of additively manufactured AlSi10Mg alloy after exposure to elevated temperatures, Materials Characterization 137, p. 119-126.

[6] Kempf, A., Hilgenberg, K., 2021. Influence of heat treatments on AlSi10Mg specimens manufactured with different laser powder bed fusion instruments, Material Science & Engineering A, Journal Pre-Proof, https://doi.org/10.1016/j.msea.2021.141371 .

[7] Beretta, S., Romano, S., 2017. A comparison of fatigue strength sensitivity to defects for materials manufactured by AM or traditional processes, International Journal of Fatigue 94, p. 178-191.